Magnetic structures of $(Co_{2-x}Ni_x)(OH)PO_4$ (x = 0.1,0.3) spin glass-like state in antiferromagnetically ordered phases

2006 J. Phys.: Condens. Matter 18 3767

(http://iopscience.iop.org/0953-8984/18/15/021)

INSTITUTE OF PHYSICS PUBLISHING JOURNAL OF PHYSICS: CONDENSED MATTER

J. Phys.: Condens. Matter **18** (2006) 3767–3787 doi:10.1088/0953-8984/18/15/021

Magnetic structures of $(Co_{2-x}Ni_x)(OH)PO_4$ ($x = 0.1, 0.3$) spin glass-like state in antiferromagnetically ordered phases

I de Pedro[1], J M Rojo[1], J L Pizarro[2], J Rodríguez Fernández[3], J Sánchez Marcos[3], M T Fernández-Díaz[4], M I Arriortua[2] and T Rojo[1,5]

[1] Departamento de Química Inorgánica, Facultad de Ciencia y Tecnología, Universidad del País Vasco, 48080 Bilbao, Spain
[2] Departamento de Mineralogía y Petrología, Facultad de Ciencia y Tecnología, Universidad del País Vasco, 48080 Bilbao, Spain
[3] CITIMAC, Facultad de Ciencias, Universidad de Cantabria, 39005 Santander, Spain
[4] Institut Laue-Langevin, BP 156X, F-38042 Grenoble Cedex, France

E-mail: teo.rojo@ehu.es

Received 28 November 2005, in final form 21 February 2006
Published 30 March 2006
Online at stacks.iop.org/JPhysCM/18/3767

Abstract

Compounds of the general formula $Co_{2-x}Ni_x(OH)PO_4$ ($x = 0.1, 0.3$) have been synthesized under mild hydrothermal conditions. Neutron powder diffraction, susceptibility and heat capacity measurements were carried out on polycrystalline samples. The cobalt–nickel compounds are ordered as three-dimensional antiferromagnets with ordering temperatures of 70 and 64 K for $x = 0.1$ and $x = 0.3$, respectively. The magnetic study shows a spin glass-like state below 11 and 5 K for $Co_{1.9}Ni_{0.1}(OH)PO_4$ and $Co_{1.7}Ni_{0.3}(OH)PO_4$, respectively. Specific heat data present peaks at 68 and 61 K for $Co_{1.9}Ni_{0.1}$ and $Co_{1.7}Ni_{0.3}$, respectively. These peaks show broad shoulders between approximately 15 and 40 K. The lack of any distinguishable anomaly below 10 K supports the spin glass nature of the low temperature transitions. Refinement of room temperature neutron diffraction data indicates that the Ni(II) ions are in octahedral co-ordination with the practical absence of these ions in the trigonal bipyramidal sites. The magnetic structures of $Co_{2-x}Ni_x(OH)PO_4$ consist of ferromagnetic arrangements between the octahedral chains and trigonal bipyramidal dimers within the xz plane with the magnetic moments along the z axis. The ferromagnetic layers are disposed antiparallel to one another along the y direction establishing the three-dimensional antiferromagnetic order ($T_N \approx 70$ K for $Co_{1.9}Ni_{0.1}$ and $\approx$64 K for $Co_{1.7}Ni_{0.3}$). The different exchange pathways, the anisotropy of the Co(II)

[5] Author to whom any correspondence should be addressed.

ions and the frustration of the magnetic moments in the trigonal bipyramidal geometry could be responsible for the freezing process.

M Supplementary data files are available from stacks.iop.org/JPhysCM/18/3767

(Some figures in this article are in colour only in the electronic version)

1. Introduction

Since spin glass (SG) behaviour was discovered in diluted magnetic alloys in the 1970s [1, 2] interest in the study of this phenomenon has steadily increased. Nowadays, many magnetic systems present macroscopic behaviour that resembles that of canonical spin glasses and the terms spin glass (SG), spin glass-like or cluster glass frequently appear in the literature [3–13]. The first kind of system to be studied widely consisted of dilute solutions of magnetic transition metal impurities in a noble metal host [14, 15]. Canella and Mydosh showed that the ac susceptibility presents a sharp cusp which is generally associated with a SG transition [16]. The appearance of SG signatures in the macroscopic properties of more concentrated magnetic systems caused controversy about the real nature of the transition due to the formation of clusters, which could interact with each other in different ways. This controversy remains in phases such as the granular giant magnetoresistance (GMR) alloys [3], perovskites [4] and Kondo compounds [5, 6]. Frustration and randomness are the basic requirements for SG, and therefore the appearance of SG behaviour in dense magnetic compounds with crystalline structures, such as URh_2Ge_2 [7] or U_2IrSi_3 [8], has attracted much attention in recent years. The term 'non-magnetic atom disorder spin glasses' has been coined for this family of materials [9].

The possible coexistence of long range magnetic order and SG behaviour with the existence of ferromagnetic spin correlations, which persist into the SG regions, has been proposed but not conclusively demonstrated [17]. The re-entrant SG behaviour, in which the material is first ferromagnetic and then, on decreasing the temperature, transforms into a SG state, has been found in crystalline [10, 11] and amorphous [12] compounds. The opposite behaviour, from SG to ferromagnetic with decreasing temperature, has recently been found in $CeNi_{1-x}Cu_x$ [13]. The coexistence of antiferromagnetism and SG has been clearly observed in disordered systems such as $Fe_{0.55}Mg_{0.45}Cl_2$ [18] and $Fe_xMn_{1-x}TiO_3$ [19] where a random distribution of Fe–Mg or Fe–Mn appears.

We have recently discovered the coexistence of AF and SG in a magnetically ordered system, the phosphate $Co_2(OH)PO_4$. This is the first three-dimensional antiferromagnetic phosphate ($T_N \approx 71$ K) with a spin glass state below $T_f \approx 15$ K [20]. This compound belongs to the mineral adamite-type $M_2(O/OH)XO_4$ (M = Zn, Mg, Mn, Co, Cu ...) (X = P, As ...) [21–27] family which exhibits a considerable number of structures that can give rise to potential applications and interesting properties such as magnetism, heterogeneous catalysis, ion exchange, optics and thermal expansion [28–30]. The hydroxyphosphate group of materials has been known for many years, but some of them have never been prepared in the laboratory as pure phases. Recently, hydrothermal techniques based on the control of temperature and pressure within the reaction medium have been shown to be a good for the attainment of pure phases [31–34]. The crystal structure of the adamite mineral $Zn_2(OH)AsO_4$ [21] can be described as being formed by two crystallographically distinct metal ions sited in two different topologies, with the octahedra $[Zn(2)O_4(OH)_2]$ giving rise to linear chains and the trigonal bipyramids $[Zn(1)O_4(OH)]$ forming dimeric entities (see figure 1). The condensed three-dimensional framework is obtained by the linking of edge-sharing $[MO_4(OH)_2]$ octahedra and distorted $[MO_4(OH)]$ trigonal bipyramids and $[XO_4]$ tetrahedra.

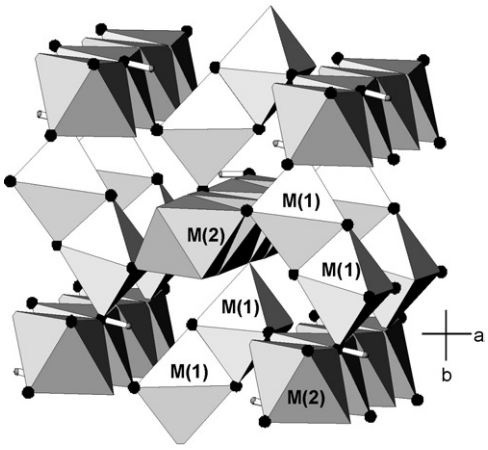

Figure 1. Polyhedral view of unit cell packing of $(Co, Ni)_2(OH)PO_4$ along the |001| direction. Light and dark polyhedra are occupied by Co(1), Co(2) and nickel ions. Tetrahedra have not been shown for clarity.

The complex magnetic behaviour in $Co_2(OH)PO_4$ is attributed to the existence of two antiferromagnetically coupled ferromagnetic dimeric and chain sublattices. The geometrical frustration, together with the anisotropy of the Co(II) ions and the magnetic exchange pathways, could be responsible for the spin glass behaviour. The substitution of Co^{2+} ($S = 3/2$) by Ni^{2+} ($S = 1$) cations should create additional randomness in the magnetic interactions and give rise to interesting variations in the magnetic properties of $Co_2(OH)PO_4$. In order to determine the nature of the main magnetic interactions in this type of compound we have studied the magnetic properties of two cobalt-substituted phosphates with the general formula: $Co_{2-x}Ni_x(OH)PO_4$.

2. Experiment

Polycrystalline $Co_{2-x}Ni_x(OH)PO_4$ ($x = 0.1, 0.3$) was synthesized hydrothermally. Stoichiometric $(Co, Ni)_3(PO_4)_2{\cdot}8H_2O$ precursors were prepared following a method previously described [35]. These hydrated cobalt–nickel phases were heated at approximately 180 °C in a 90% filled Teflon-lined stainless steel autoclave [32]. It has been verified that the highest degree of nickel substitution obtained was approximately 15%. The contents of cobalt, nickel and phosphorus were determined by inductively coupled plasma atomic emission spectroscopy (ICP-AES) performed with an ARL Fisons 3410 spectrometer and were consistent with the $Co_{1.9}Ni_{0.1}(OH)PO_4$ and $Co_{1.7}Ni_{0.3}(OH)PO_4$ stoichiometries.

Room temperature x-ray powder diffraction data were obtained in the $10° \leqslant 2\theta \leqslant 90°$ range in steps of 0.02° with an integration time of 16 s per step using a Philips X'Pert-MPD x-ray diffractometer with secondary beam graphite monochromated Cu Kα radiation. Neutron powder diffraction data were collected at 2 and 298 K on Instrument D2B at the Institut Laue–Langevin (ILL), Grenoble, France. Thermal neutrons were incident on 5 g of polycrystalline $Co_{2-x}Ni_x(OH)PO_4$ ($x = 0.1, 0.3$) compounds, packed in a cylindrical vanadium container and held in a liquid helium cryostat. The high resolution of D2B was used to obtain structural data for $Co_{1.7}Ni_{0.3}(OH)PO_4$ at room temperature over a large angular range $10° \leqslant 2\theta \leqslant 150°$ in steps of 0.05° with an integration time of 50 000 monitor counts per step and with each point in the diffraction pattern being recorded by six independent detectors for subsequent

normalization and summation, giving an overall collection time of approximately 3 h for the entire data set.

Temperature dependent neutron powder diffraction data were collected on Instrument D1B at the ILL. Data were collected every 5 K from 1.8 to 100 K over the angular range $10° \leqslant 2\theta \leqslant 90°$. D1B has a 400-element linear multidetector spaced every 0.2° covering an angular range of 80°, which allowed measurement of the magnetic peaks. This enabled the magnetic structures to be determined throughout the entire temperature region of interest. The Rietveld method [36] was used to refine the crystal and magnetic structures. All the data, from x-ray as well as from neutron diffraction, were analysed using the FULLPROF [37] program suite. The magnetic and nuclear structures were refined simultaneously. The background was fitted to a polynomial refinable function. The D1B patterns were refined sequentially, taking as the starting parameters of each pattern those resulting from the refinement of the preceding one. A pseudo-Voigt function was chosen to generate the line shape of the diffraction peaks.

DC magnetic susceptibility measurements of powdered samples were performed using a Quantum Design MPSM-7 SQUID magnetometer whilst heating from 4.2 to 300 K in an applied magnetic field of 1 kOe, after cooling either in the presence (field cooling, FC) or absence (zero field cooling, ZFC) of the applied field. Magnetization as a function of field (H) was measured using the same MPSM-7 SQUID magnetometer in the range $-70 \leqslant \mathrm{H/kOe} \leqslant 70$ in the temperature range of 5–100 K after cooling the sample in zero field. AC magnetic susceptibility measurements were made using a standard Quantum Design Physical Property Measurement System (PPMS) with an alternating excitation field (H_{ac}) of 1 Oe. Data were recorded from 1.8 to 100 K as a function of both frequency and applied DC magnetic field. Frequencies between 10 and 10^4 Hz were measured in the absence of an applied field and field dependent data were collected at a fixed frequency of 1000 Hz with applied fields from 0 to 2 kOe. Heat capacity measurements were carried out by a two-tao relaxation method using the same PPMS system. The sample was a plate of thickness 0.3 mm and ≈5 mg weight obtained by compressing the original polycrystalline powder. Data were collected with zero field and under an applied field of 90 kOe from 1.8 to 150 K. The phonon contribution, modelled by two independent Debye spectra, was subtracted to give the magnetic specific heat, $C_{p_{\mathrm{mag}}}$.

3. Results

3.1. Room temperature structure

The x-ray powder diffraction data were used to evaluate the purity of the products obtained in the synthesis. No unindexed diffraction peaks were observed in the final refinements, leading to the conclusion that the results obtained correspond to pure phases. To study the crystal structure of $Co_{1.7}Ni_{0.3}(OH)PO_4$, the room temperature D2B powder neutron diffraction pattern was refined using the Rietveld method, taking as starting models the x-ray single crystal data of $Co_2(OH)PO_4$ reported in [26]. The observed, calculated and difference neutron powder diffraction data for $Co_{1.7}Ni_{0.3}(OH)PO_4$ are shown in figure 2. The room temperature structural parameters and the reliability factors from D2B data refinements are summarized in table 1. There is no significant mismatch between the observed intensity and the calculated profile, which is generated from the model crystal structure in table 1. The data obtained from the Rietveld fits at 2 and 100 K of $Co_{1.7}Ni_{0.3}(OH)PO_4$ are similar to those of the room temperature structure. These results are in agreement with those obtained for the unsubstituted phase, $Co_2(OH)PO_4$ [20].

No high resolution D2B neutron diffraction data were available for $Co_{1.9}Ni_{0.1}(OH)PO_4$, but using the D1B data at 100 K and from the previous study of $Co_{1.7}Ni_{0.3}(OH)PO_4$, reasonable

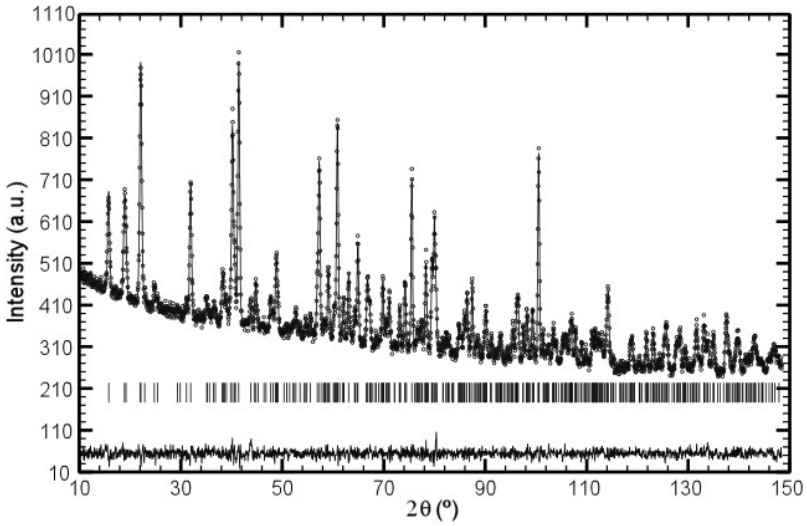

Figure 2. Observed (circles), calculated (solid line) and difference (at the bottom) neutron diffraction (D2B, ILL) profiles of $Co_{1.7}Ni_{0.3}(OH)PO_4$ at room temperature. The tick marks denote allowed crystal structure reflections.

Table 1. Details of Rietveld refinements from neutron diffraction patterns at room temperature and 100 K for $Co_{2-x}Ni_x(OH)PO_4$ ($x = 0.1, 0.3$), respectively.

Compound	$Co_{1.7}Ni_{0.3}(OH)PO_4$	$Co_{1.7}Ni_{0.3}(OH)PO_4$	$Co_{1.9}Ni_{0.1}(OH)PO_4$
Space group	*Pnnm* (No. 58)	*Pnnm* (No. 58)	*Pnnm* (No. 58)
a (Å)	8.0206(2)	8.008(1)	8.030(1)
b (Å)	8.3646(2)	8.365(2)	8.386(2)
c (Å)	5.9403(1)	5.937(1)	5.952(1)
V (Å^3)	398.53(1)	397.7(2)	400.8(1)
Instrument	D2B (ILL)	D1B (ILL)	D1B (ILL)
T (K)	300	100	100
Radiation (Å)	1.5938	2.525	2.525
Monochromator	Ge(335)	Ge(311)	Ge(311)
Z	4	4	4
2θ range (deg)	10–148.5	10–84	10–84
2θ step-scan increment (deg)	0.05	0.2	0.2
No. of reflections	403	39	39
No. of parameters	71	26 [a]	42
Reliability factor (%)			
$R_p = \Sigma\lvert y_{i,\mathrm{obs}} - (1/c)\ y_{i\mathrm{calc}}\rvert/\Sigma y_{i,\mathrm{obs}}$	14.0	23.8	23.2
$Rw_p = [\Sigma w_i\lvert y_{i,\mathrm{obs}} - (1/c)y_{i,\mathrm{calc}}\rvert^2/\Sigma w_i[y_{i,\mathrm{obs}}]^2]^{1/2}$	12.1	14.8	14.0
$R_\mathrm{B} = [\Sigma\lvert I_\mathrm{obs} - I_\mathrm{calc}\rvert/\Sigma I_\mathrm{obs}$	3.8	6.1	4.96
χ^2	1.11	1.30	1.23

[a] Atomic co-ordinates were not refined.

refinements of the nuclear structure of the $Co_{1.9}Ni_{0.1}$ compound were obtained (see table 1). The phases show small differences in the lattice parameters due to the larger radius of the Co^{2+} ions.

Table 2. Main magnetic data of the $Co_{2-x}Ni_x(OH)PO_4$ ($x = 0$, 0.1 and 0.3) hydroxyphosphates.

Compound	T_N (K)	T_f (K)	C_m (cm^3 K mol^{-1})	θ (K)	μ_{eff} (μ_B) $T = 300$ K	m (μ_B)[a] $T \sim 2$ K M(1)	M(2)	Ref.
$Co_2(OH)PO_4$	71	15	3.59	−63.5	5.36	3.39	3.84	[20]
$Co_{1.9}Ni_{0.1}(OH)PO_4$	70	11	3.21	−57.6	5.07	2.91	3.56	This work
$Co_{1.7}Ni_{0.3}(OH)PO_4$	64	5	2.63	−48.3	4.59	2.93	3.19	[32], this work

[a] From neutron diffraction.

In the $Co_{1.7}Ni_{0.3}(OH)PO_4$ compound, the M(2) atoms exhibit an elongated octahedral geometry with two long apical bond distances, M(2)–O(3)[i] of 2.254(2) Å, and four shorter equatorial links, M(2)–O(2) of 2.078(4) Å and M(2)–O(4)H of 2.015(4) Å in the *cis* configuration (supplementary material available at stacks.iop.org/JPhysCM/18/3767). O(1), O(2) and O(3) atoms bond to two metal (Co, Ni) ions and one phosphorus atom, while O(4) is linked to three distinct metal ions, as well as to a proton (OH group). The M(1) atoms are fivefold coordinated by oxygen atoms in an approximately trigonal bipyramidal geometry. The equatorial M(1)–O(1)[ii] and M(1)–O(3) bond distances are 2.096(6) Å and 2.011(4) Å, respectively, whereas the apical M(1)–O(1)[iii] and M(1)–O(4)H bond distances are 1.988(6) and 2.027(8) Å, respectively. The axial and equatorial O–M(2)–O mean angles in the MO_6 octahedra are 170.5° and 91.9°. For the MO_5 polyhedra, each trigonal bipyramid exhibits three sets of O–M(1)–O angles around 90°, 120° and an axial one to 167.6°. Finally, in both $Co_{2-x}Ni_x(OH)PO_4$ ($x = 0.1$, 0.3) phases, the phosphate groups exhibit three different bond lengths and four different bond angles with mean distances and angles of 1.54(1) Å and 108.8°, respectively, showing quite regular PO_4 groups (supplementary material available at stacks.iop.org/JPhysCM/18/3767). The bond distances and angles obtained for $Co_{1.7}Ni_{0.3}$ and $Co_{1.9}Ni_{0.1}$ are in good agreement with those of $Co_2(OH)PO_4$ [26].

3.2. Magnetic properties

The temperature and field dependences of the magnetic susceptibility and the magnetization of $Co_{2-x}Ni_x(OH)PO_4$ ($x = 0.1$, 0.3) have been investigated. Some aspects of the magnetic behaviour of the $x = 0.3$ phase were previously described in [32], and these data are shown for comparison in table 2. At first glance, the thermal behaviour of the magnetic susceptibility of both Co–Ni phases seems to be similar to that of $Co_2(OH)PO_4$ [20]. An antiferromagnetic ordering at about 65 K, obeying a Curie–Weiss law at temperatures higher than 150 K, was observed. Magnetic measurements under a magnetic field of 1 kOe for both substituted phases show a continuous decrease in the effective magnetic moment from room temperature to 4.2 K (see figure 3 and table 2). The Curie–Weiss parameters and the position of the χ_m maxima in both Co–Ni phases are lower than in $Co_2(OH)PO_4$, as should be expected due to the substitution of Co^{2+} ($S = 3/2$) by Ni^{2+} ($S = 1$). The negative Weiss constant, together with the continuous decrease in the $\chi_m T$ versus T curves, implies that the dominant interactions between neighbouring magnetic ions are antiferromagnetic. At low temperatures ($T < 20$ K) another strong magnetic signal below 10 K appears in both $Co_{2-x}Ni_x(OH)PO_4$ ($x = 0.1$, 0.3) compounds, indicating the possible existence of a new magnetic state below this temperature.

More detailed experiments have shown irreversibility effects in the magnetic susceptibility below the ordering temperature (T_N) (see figure 3). Above T_N, a paramagnetic behaviour without any difference between ZFC and FC magnetization is observed in both Co–Ni hydroxyphosphates. The FC and ZFC magnetization curves start to separate at around T_N (∼65 K), where a significant irreversibility begins to develop. These results are quite different

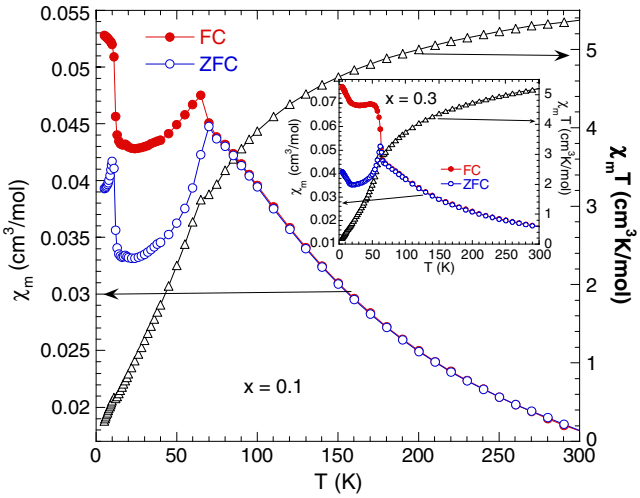

Figure 3. Thermal evolution of the molar magnetic susceptibility (χ_m) in field cooled (FC) and zero field cooled (ZFC) modes together with the $\chi_m T$ product at 1 kOe for $Co_{1.9}Ni_{0.1}(OH)PO_4$. The inset shows the same properties for $Co_{1.7}Ni_{0.3}(OH)PO_4$.

from those observed for the non-substituted $Co_2(OH)PO_4$ phase in which the irreversibility only appears below its freezing temperature ($T_f \approx 15$ K). So, the different magnetic behaviour observed in the FC and ZFC curves in the substituted phases can be attributed to the presence of magnetic cations with distinct spins. The main differences in the ZFC curves at lower temperatures are observed below 20 K where a maximum appears near 10 K for $Co_{1.9}Ni_{0.1}(OH)PO_4$ and only a minimum appears at around 15 K in $Co_{1.7}Ni_{0.3}$.

The temperature dependence of the remanent magnetization of $Co_{1.9}Ni_{0.1}(OH)PO_4$ between 4.2 and 100 K presents a similar behaviour to that observed in $Co_{1.7}Ni_{0.3}(OH)PO_4$ [32]. The remanent magnetization curves in both hydroxyphosphates at $H_{dc} = 0$ after cooling from $T > T_N$ under a magnetic field of 1 kOe diminish to zero above 70 and 64 K for $Co_{1.9}Ni_{0.1}$ and $Co_{1.7}Ni_{0.3}$, respectively. This dependence is characteristic of a paramagnetic state. Below these temperatures, the remanent magnetization strongly increases up to approximately 7 emu mol^{-1} for $Co_{1.9}Ni_{0.1}$ and 12 emu mol^{-1} for $Co_{1.7}Ni_{0.3}$ at 40 K, higher than the value of 5 emu mol^{-1} obtained for $Co_2(OH)PO_4$ [20] (see figure 4). Therefore, the ferromagnetic component between 65 and 40 K increases with the Ni content, indicating the important effect of the small spin change (Co^{2+} ($S = 3/2$) by Ni^{2+} ($S = 1$) ions) in the magnetic behaviour. Both substituted compounds show a continuous increase of the remanent magnetization with decreasing temperature up to 10 K (∼8 emu mol^{-1}) and 15 K (∼12.54 emu mol^{-1}) for $Co_{1.9}Ni_{0.1}$ and $Co_{1.7}Ni_{0.3}$, respectively. Below these inflection points, a new greater increase of the remanent magnetizations is also observed. Although the Co–Ni phases did not show a clear maximum at $T < 20$ K as in $Co_2(OH)PO_4$, these behaviours point again toward the presence of a new magnetic state below 10 K. The thermoremanent behaviour together with the irreversibility are characteristic of a weak ferromagnetic component [32] which was not observed from the neutron diffraction data, as we will see later. It is worth mentioning that a canted antiferromagnetic structure showing irreversibility was also observed in a hydroxy Fe(III) phosphate. This irreversibility was attributed to the formation of magnetic domains and domain-wall movement [38].

The ac magnetic susceptibility measurements of $Co_{1.9}Ni_{0.1}(OH)PO_4$ were carried out with an alternating excitation field of 1 Oe and a frequency of 10^3 Hz. The results are shown in

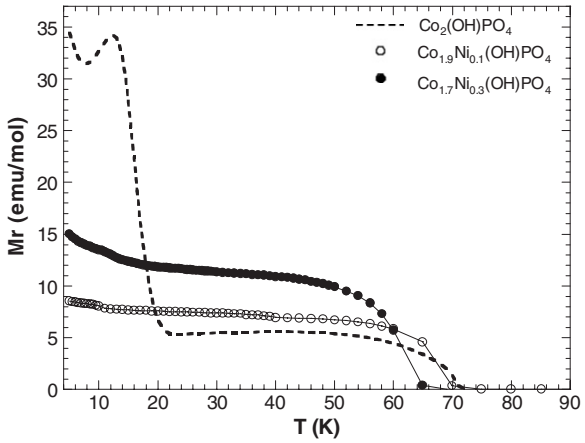

Figure 4. Temperature dependence of the thermoremanent magnetization between 4.2 and 100 K for $Co_{2-x}Ni_x(OH)PO_4$ ($x = 0.1, 0.3$). The TRM curve of $Co_2(OH)PO_4$ is also shown for comparison.

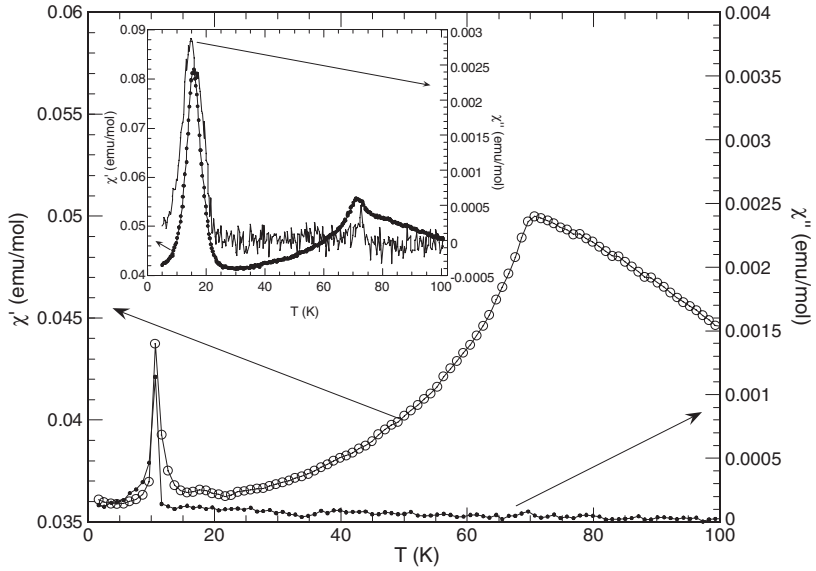

Figure 5. Real (χ') and imaginary (χ'') part of the magnetic susceptibility of $Co_{1.9}Ni_{0.1}(OH)PO_4$ in a driving field of 1 Oe. The inset shows the ac susceptibility of $Co_2(OH)PO_4$ in $H_{ac} = 1$ Oe and $\nu = 100$ Hz.

figure 5. As was observed in $Co_{1.7}Ni_{0.3}(OH)PO_4$ [32], the presence of a shark peak at low temperatures associated with the spin glass transition is also detected in $Co_{1.9}Ni_{0.1}(OH)PO_4$. The thermal evolution of the real (or in-phase, χ') component of the susceptibility near 65 K for both Co–Ni compounds is similar to that observed in $Co_2(OH)PO_4$ (see inset in figure 5) and is attributed to the existence of long range order interactions. The lack of absorption in the imaginary (or out-of-phase, χ'') component in this temperature region indicates the presence of an antiferromagnetic order, in good agreement with the results obtained from the molar magnetic susceptibility data and the magnetic behaviour observed for $Co_2(OH)PO_4$ [20].

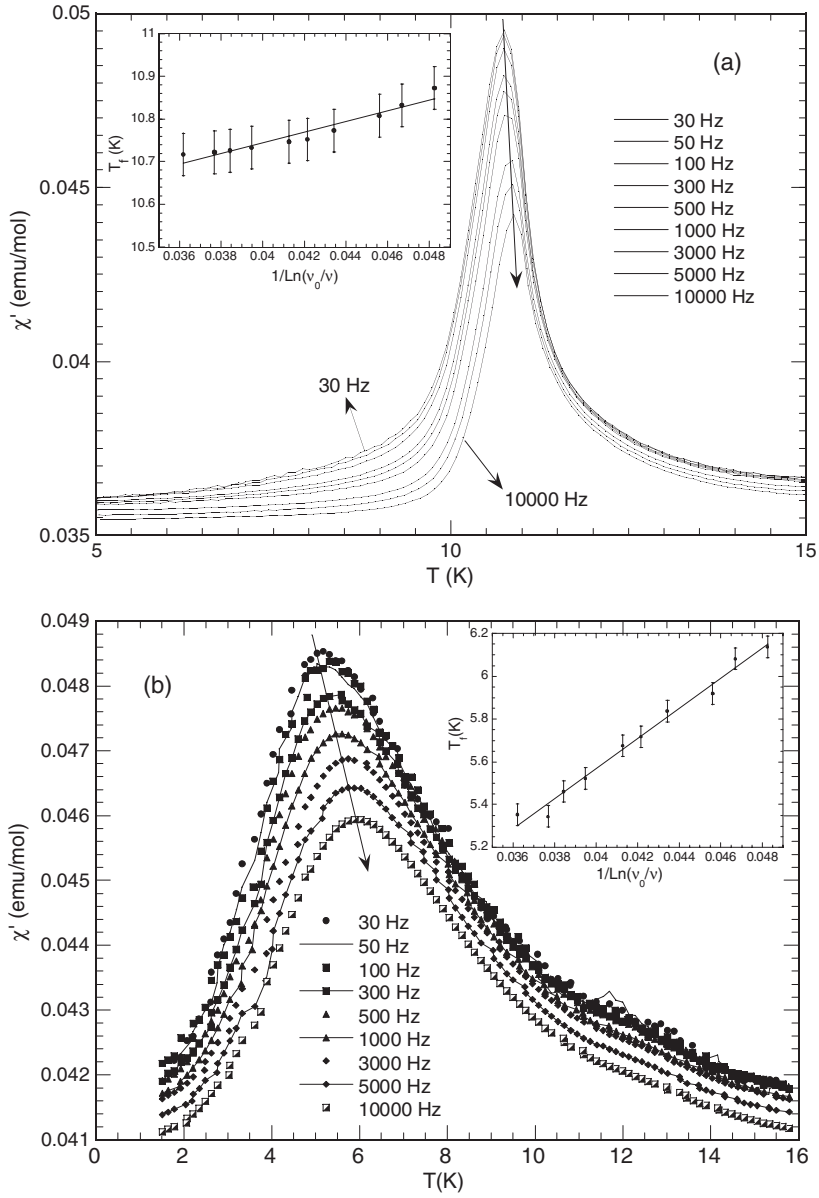

Figure 6. AC (χ') susceptibility curves of (a) $Co_{1.9}Ni_{0.1}(OH)PO_4$ and (b) $Co_{1.7}Ni_{0.3}(OH)PO_4$ for different excitation frequencies. The insets show a fit of the position of the susceptibility maximum to a Vogel–Fulcher law.

Furthermore, the strong peaks observed in both χ' and χ'' at 11 and 5 K for $Co_{1.9}Ni_{0.1}$ and $Co_{1.7}Ni_{0.3}$, respectively, indicate the existence of a magnetic transition of a different nature from that at the high temperature.

The results of the χ' variation for $Co_{2-x}Ni_x(OH)PO_4$ ($x = 0.1, 0.3$) at different frequencies are shown in figure 6. This peak shifts to higher temperatures with increasing frequency, precluding long range magnetic order as the origin of this transition. The frequency

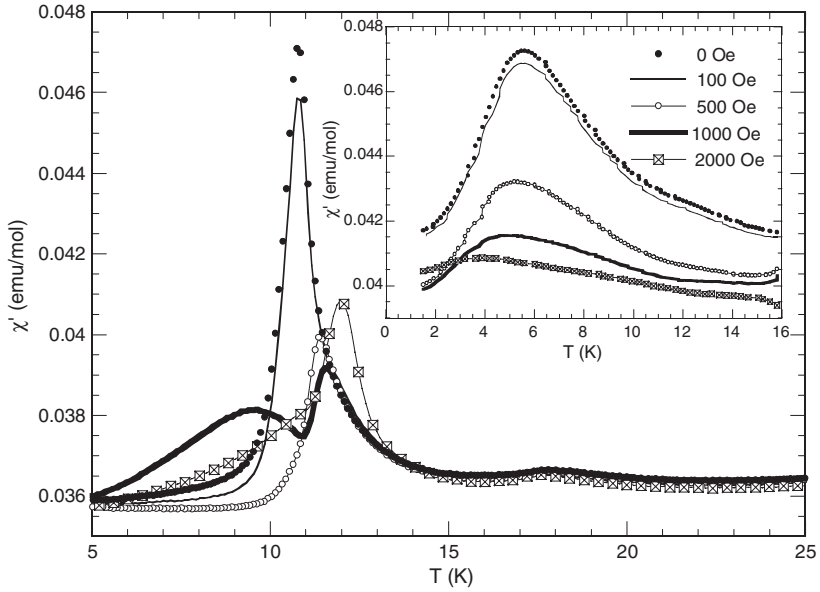

Figure 7. AC susceptibility (χ') versus temperature (T) at different magnetic fields in the region of the spin glass transition for $Co_{1.9}Ni_{0.1}(OH)PO_4$. The inset shows the ac susceptibility of $Co_{1.7}Ni_{0.3}(OH)PO_4$.

dependence is characteristic of spin glasses in which the cooperative freezing of individual magnetic moments occurs at the freezing temperature T_f, defined as that corresponding to the maximum in χ' [2]. The dependence of T_f with frequency is shown in the insets of figure 6 where the in-phase χ' components follow an empirical Vogel–Fulcher law.

The effect of a superimposed dc field on χ' in the low temperature region is shown in figure 7. The ac susceptibility for $Co_{2-x}Ni_x(OH)PO_4$ ($x = 0.1, 0.3$) shows a clear dependence on magnetic field. In the $Co_{1.9}Ni_{0.1}$ compound, the χ' susceptibility peak decreases with increasing magnetic field up to 750 Oe where the signal is split. Higher magnetic fields cause wide bands which do not disappear with the field. However, in the $Co_{1.7}Ni_{0.3}$ phase [32], the peak is shifted with increasing magnetic field (see inset in figure 7) disappearing at about 2000 Oe. This last behaviour is in good agreement with that observed in $Co_2(OH)PO_4$ [20] which is consistent with the existence of a spin glass transition. On the other hand, the persistence of the peak in the $Co_{1.9}Ni_{0.1}$ phase is quite unusual, reflecting a more complex magnetic behaviour than that induced by the magnetic field in a canonical spin glass-like state.

The specific heat measurements of $Co_{2-x}Ni_x(OH)PO_4$ ($x = 0.1, 0.3$) between 1.8 and 150 K are shown in figure 8. The heat capacity data exhibit three-dimensional magnetic ordering peaks at 68 and 61 K for the $Co_{1.9}Ni_{0.1}$ and $Co_{1.7}Ni_{0.3}$ phases, respectively. The temperatures at which these peaks appear are consistent with those obtained from the magnetic susceptibility measurements. At temperatures higher than ∼80 K for both Co–Ni compounds, the strong increases of C_p are due to the lattice (or phonon) contribution ($C_{p_{pho}}$). Below this temperature the magnetic contribution ($C_{p_{mag}}$) is relatively significant compared with the phonon one. In the absence of non-magnetic isostructural compounds, the contribution of the lattice vibrations to the specific heat capacity was fitted to the high temperature data by a Debye model [39] by considering the existence of two-phonon spectra [20]. For the unit cell containing N atoms, n_1 was assigned a Debye temperature θ_1 and n_2, constrained such that $n_2 = N - n_1$, a

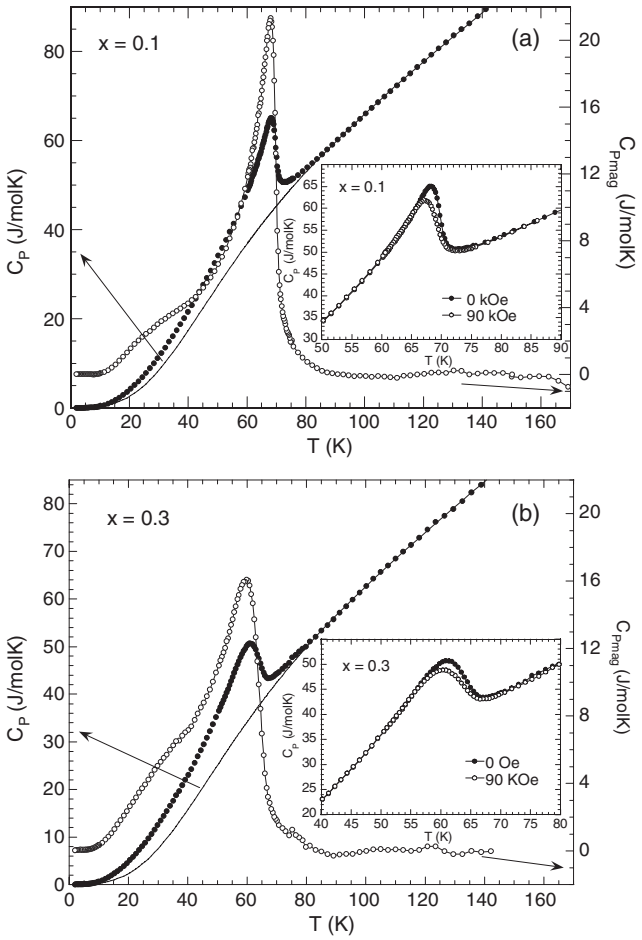

Figure 8. Specific heats for (a) $Co_{1.9}Ni_{0.1}(OH)PO_4$ and (b) $Co_{1.7}Ni_{0.3}(OH)PO_4$. Full points represent the (C_p) experimental data and the full line the ($C_{p_{pho}}$) estimated phonon contribution. The circles show the calculated ($C_{p_{mag}}$) magnetic contribution after subtracting the phonon contribution. The inset shows the specific heat of $Co_{2-x}Ni_x(OH)PO_4$ ($x = 0.1$ and 0.3) at 0 and 90 kOe.

Debye temperature θ_2, yielding three independent variables to be refined, namely θ_1, θ_2 and n_1. The experimental data above the ordering temperatures were fitted to this phenomenological model for both Co–Ni compounds. Continuous lines in figures 8(a) and (b) show the best fits. The refined values are shown in table 3. The obtained parameters are in good agreement with the unit cell contents of three heavy atoms and six light atoms with a higher Debye temperature. The estimated Debye temperature associated with the dynamics of the three heaviest elements (θ_2) in both hydroxyphosphates is similar, due to the fact that Co and Ni have similar atomic masses.

The contribution of the experimental magnetic heat capacity ($C_{p_{mag}}$) in each cobalt–nickel compound was obtained by subtracting the phonon contribution from the measured specific heat (see figure 8). In addition to the λ-type peak at the ordering temperature, a shoulder can also be observed at around 35 K for both Co–Ni phases which can be attributed to a spin glass-like behaviour where a broad anomaly in $C_{p_{mag}}$ usually appears at temperatures higher than the freezing temperature [1].

Table 3. Summary of specific heat data of the $Co_{2-x}Ni_x(OH)PO_4$ ($x = 0$, 0.1 and 0.3) compounds.

$Co_{2-x}Ni_x(OH)PO_4$	$x = 0$[a]	$x = 0.1$	$x = 0.3$
T_{max} (K)	70	68	61
Inflection point (K)	71	70	64
$C_{m\,max}$ (J K^{-1} mol^{-1})	18.7	21.4	16.2
Width at half-height C_m (K)	10	9.8	19
Debye model			
Range of fit (K)	80–140	80–140	80–140
n_1	6.2	6.1	6.0
θ_1 (K)	1001	1010	1032
θ_2 (K)	232	238	250

[a] Graphical representation (C_p, $C_{p_{pho}}$, $C_{p_{mag}}$) is given in [20].

The effect of the magnetic field on the heat capacity has also been studied. The thermal evolution of the specific heat of $Co_{2-x}Ni_x(OH)PO_4$ ($x = 0.1$, 0.3) is shown in the inset of figure 8. It can be observed that the heat capacity is not significantly affected by the applied magnetic field over the whole temperature range, even up to 90 kOe, with only a small shift of the lambda anomaly to lower temperature, characteristic of antiferromagnetic behaviour, being observed. The robustness of the magnetic transition against the magnetic field reflects the strong magnetic anisotropy of these materials.

3.3. Low temperature neutron diffraction

3.3.1. Magnetic structure refinements. The D1B neutron diffraction patterns at 1.8 K for $Co_{2-x}Ni_x(OH)PO_4$ ($x = 0.1$, 0.3) are represented in figure 9. Rietveld refinements of the low temperature crystal structures showed that the *Pnnm* symmetry is maintained down to 1.8 K. The patterns exhibit additional magnetic peaks, indicating that both compounds are magnetically ordered at low temperatures. All magnetic peaks were indexed with a propagation vector $k = (0, 0, 0)$ referenced to the room temperature unit cell, indicating that the magnetic and nuclear unit cells are equal. The thermal evolution of the D1B diffraction patterns for both Co–Ni hydroxyphosphates was followed from 1.8 to 100 K. It is worth noting that a very intense reflection appears at $d \sim 8.40$ Å and $d \sim 8.375$ Å for $Co_{1.9}Ni_{0.1}$ and $Co_{1.7}Ni_{0.3}$, respectively. These magnetic (010) and (100) peaks arise from long range antiferromagnetic order in the samples (see figure 9).

Following the method described in [40], and taking into account the magnetic structure of $Co_2(OH)PO_4$ [20], both magnetic structures were refined. The best fits of the D1B experimental patterns for $Co_{2-x}Ni_x(OH)PO_4$ ($x = 0.1$, 0.3) at 1.8 K are plotted in figure 9. The magnetic atoms occupy two different sites, where the M(1) atoms (named R) are in the 4g position and the M(2) atoms (named S) are in the 4f position. These two sublattices generate two dimers (R1–R2) and (R3–R4) and two chains (–S1–S2–) and (–S4–S3–) (see figure 10). The ordering of the magnetic moments from the two sublattices in the unit cell, compatible with the symmetry operations, is shown in figure 10. In both Co–Ni compounds, the refinement of the components from the magnetic moments gives $M_x = 0$ and $M_y = 0$, indicating that they lie in the z direction. The magnetic discrepancy factors are $R_{mag} = 6.13$ and $R_{mag} = 4.55$ for $Co_{1.9}Ni_{0.1}$ and $Co_{1.7}Ni_{0.3}$, respectively. The saturated magnetic moments (M_z) of the [M(1)] dimer and [M(2)] chain sublattices are given in table 2.

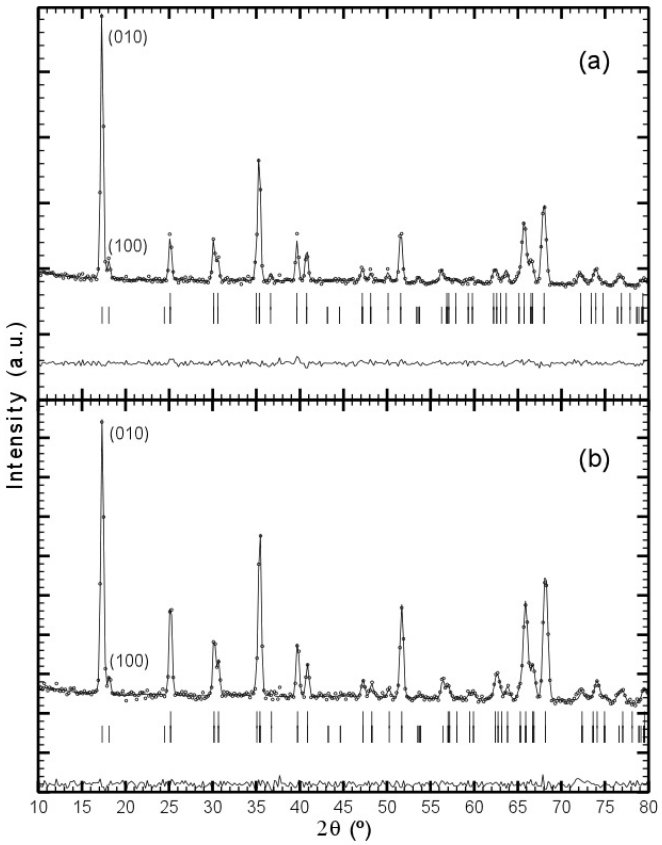

Figure 9. Refinement of D1B neutron diffraction profiles at 1.8 K of (a) $Co_{1.9}Ni_{0.1}(OH)PO_4$ and (b) $Co_{1.7}Ni_{0.3}(OH)PO_4$ ($\lambda = 2.525$ Å). The positions of the Bragg reflections for the nuclear (first row) and magnetic (second row) structures are presented. The difference curves are plotted at the bottom of the figures.

4. Thermal evolution of the ordered magnetic moments

The temperature dependent D1B diffraction data for $Co_{2-x}Ni_x(OH)PO_4$ ($x = 0.1, 0.3$) are shown in figure 11. The extra magnetic peaks generated by the antiferromagnetic long range ordering in the samples appear at around 70 K, a similar temperature to that obtained from the specific heat measurements. The higher value of the three-dimensional magnetic ordering temperature for $Co_2(OH)PO_4$ ($T_N = 71$ K) with respect to $Co_{1.9}Ni_{0.1}(OH)PO_4$ ($T_N = 70$ K) and $Co_{1.7}Ni_{0.3}(OH)PO_4$ ($T_N = 64$ K) is in good agreement with the higher spin number in Co^{2+} ($S = 3/2$) than in Ni^{2+} ($S = 1$). The intensity of the magnetic reflections in both Co–Ni phases rapidly increases, reaching a maximum at around 40 K which is practically constant down to 1.8 K.

The thermal dependences of the magnitude of the magnetic moments for $Co_{2-x}Ni_x(OH)PO_4$ ($x = 0.1, 0.3$) are represented in figure 12. It can be observed that in both Co–Ni hydroxyphosphates the three-dimensional magnetic order begins near 70 K, the ordering temperatures being similar in both sublattices. The M(2) refined magnetic moment is higher than that of the M(1) over the temperature range studied, and both curves seem to in-

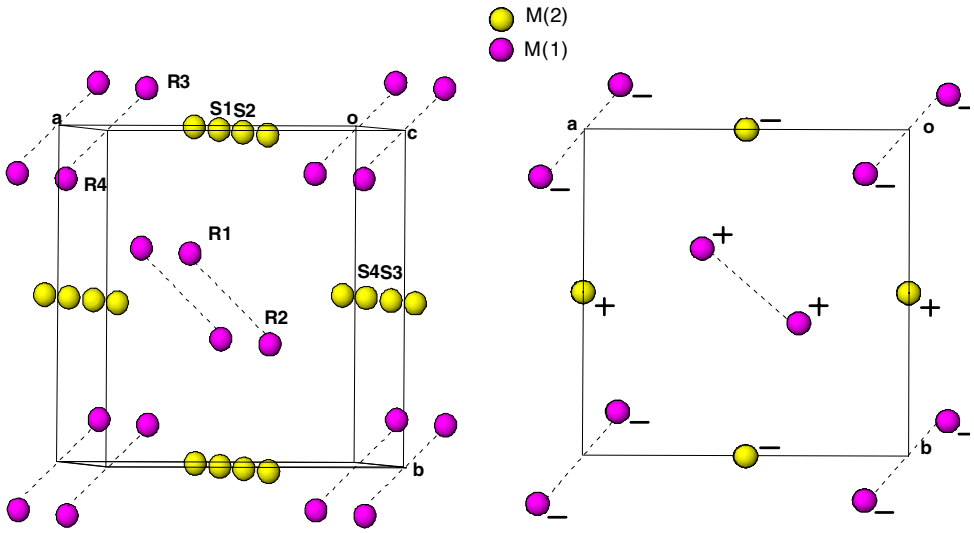

Figure 10. Projection of the magnetic structures in the (100) plane. Black and grey spheres represent the two types of M(Co, Ni) crystallographic ions. The directions of the electronic spins in the c direction are marked. Symmetry code: $R(1) = x, y, 1/2$; $R(2) = -x, -y, 1/2$; $R(3) = 1/2 + x, 1/2 - y, 0$; $R(4) = 1/2 - x, 1/2 + y, 0$; $S(1) = 1/2, 0, z$; $S(2) = -1/2, 0, -z$; $S(3) = 0, 1/2, 1/2 + z$; $S(4) = 0, 1/2, 1/2 - z$.

dicate the importance of the contribution of the octahedral chains on the overall magnetic moment. In $Co_{1.9}Ni_{0.1}(OH)PO_4$, the magnetic moment for M(2) ions slowly increases with linear variation from 3.43(4) μ_B at 40 K to 3.54(4) μ_B at 2 K, reaching the saturation value at 30 K. For the M(1) cations in the dimer groups, the magnetic moment increases from 1.71(5) μ_B at 60 K to 3.01(6) μ_B near 8 K where the saturation value is reached (see figure 12(a)). In $Co_{1.7}Ni_{0.3}(OH)PO_4$ the M(1) magnetic component continuously increases from 2.65(6) μ_B at 30 K to 2.96(6) μ_B at 2 K, whereas the magnetic moment for M(2) ions in the chains is practically linear reaching a value of 3.14(4) μ_B at 2 K (see figure 12(b)). The main magnetic differences observed between $Co_{1.9}Ni_{0.1}$ and $Co_{1.7}Ni_{0.3}$ hydroxyphosphates can be attributed to the number of Ni(II) ions in the octahedral sites.

5. Discussion and conclusion

The crystal structure of the $Co_{2-x}Ni_x(OH)PO_4$ phases is characterized by the condensed network of vertex- and edge-sharing $|MO_5|$, $|MO_6|$ and $|XO_4|$ subunits. Of the two crystallographically distinct metal atoms, M(1) is fivefold coordinated by oxygen atoms in approximately trigonal bipyramidal geometry and M(2) exhibits a distorted octahedral geometry. By edge-sharing, the octahedra give rise to linear chains propagating along the c-axis, whereas the trigonal bipyramids constitute dimeric entities. The distribution of the Ni(II) cations in the two different environments would be expected to affect the physical properties. The results of the structural refinement of the $Co_{1.7}Ni_{0.3}(OH)PO_4$ compound at room temperature show a strong preference (>97%) of the Ni(II) ions for the hexacoordinated position. In $Co_{1.9}Ni_{0.1}$, all the Ni(II) cations are located on the M(2) sites. So, considering that these values are between the error limit of the measurements, M(2) has been assumed as the only site for Ni(II).

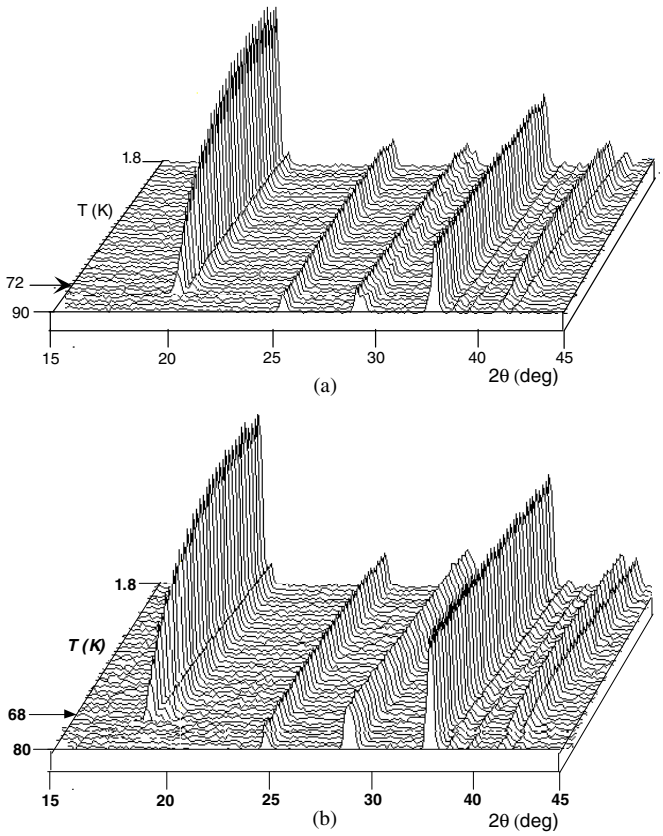

Figure 11. Thermal evolution of the neutron diffraction patterns of (a) $Co_{1.9}Ni_{0.1}(OH)PO_4$ and (b) $Co_{1.7}Ni_{0.3}(OH)PO_4$.

The magnetic study of $Co_{2-x}Ni_x(OH)PO_4$ ($x = 0.1, 0.3$) shows three-dimensional antiferromagnetic order at around 65 K for both compounds. A deeper study following the temperature, frequency and field dependences of the magnetic ac susceptibility reveals the presence of spin glass transitions at 11 and 5 K for $Co_{1.9}Ni_{0.1}$ and $Co_{1.7}Ni_{0.3}$, respectively. The strong magnetic irreversibility observed in the ZFC–FC curves at all temperatures below T_N ($\sim$65 K) for both Co–Ni phases is clearly different from that observed in $Co_2(OH)PO_4$, where the weak irreversibility starts at the freezing temperature ($T_f \approx 15$ K) due to the spin glass state. The introduction of Ni(II) ($S = 1$) ions plays an important role in both the irreversibility process and the spin glass-like state [32]. In both Co–Ni phases, the difference between the FC and ZFC curves is explained by the blocking of the magnetic moments in a paramagnetic state during the ZFC mode [1, 41, 42]. As observed in $Co_2(OH)PO_4$ [20], the magnetic irreversibility in the substituted phases decreases when the applied magnetic field increases. Moreover, the magnetization versus magnetic applied field curves of $Co_{2-x}Ni_x(OH)PO_4$ ($x = 0.1, 0.3$) show the existence of very weak hysteresis loops with small coercivity values as commonly observed in other spin glasses [20, 32, 42]. The remanent magnetization shows a ferromagnetic component for $Co_{1.7}Ni_{0.3}$ (substituted at about 15% of the Co^{2+} ($S = 3/2$) by Ni^{2+} ($S = 1$) ions) that is twice as intense as that obtained for $Co_2(OH)PO_4$. This fact, together with the continuous increase of the remanent magnetization with decreasing temperature, indicates the

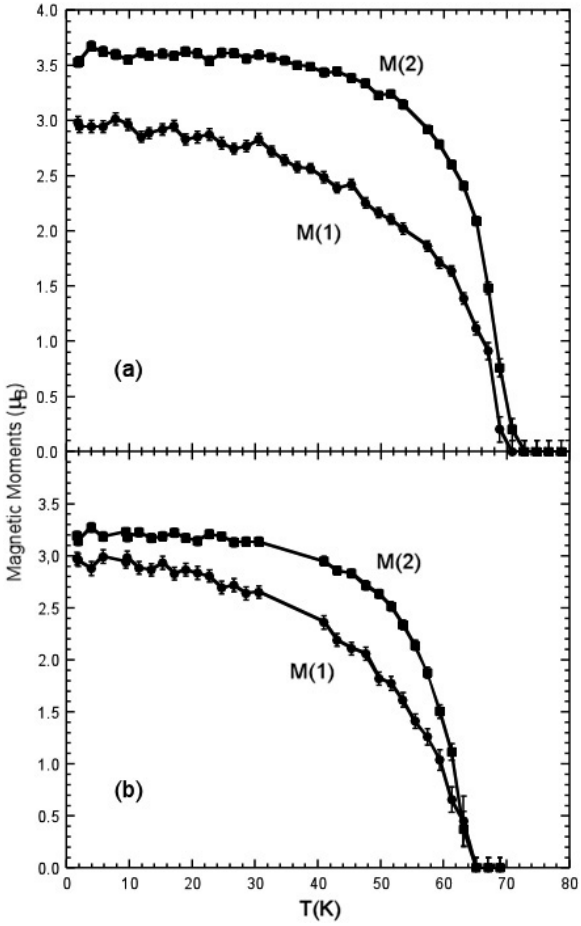

Figure 12. Magnitude of the magnetic moments of M(1) and M(2) sublattices in (a) $Co_{1.9}Ni_{0.1}(OH)PO_4$ and (b) $Co_{1.7}Ni_{0.3}(OH)PO_4$ as a function of temperature.

effect of the spin decompensations and their important role in the irreversibility observed in the dc magnetic susceptibility.

The presence of a spin glass transition in $Co_{2-x}Ni_x(OH)PO_4$ ($x = 0.1, 0.3$) is clearly observed in the ac measurements from the data obtained at different frequencies and applied fields. The initial susceptibility at the lowest frequency measured (30 Hz) shows a cusp in both Co–Ni phases (see figure 6) which has been considered as the spin glass freezing temperature ($T_f \approx 11$ K and $T_f \approx 5$ K for $Co_{1.9}Ni_{0.1}$ and $Co_{1.7}Ni_{0.3}$, respectively). In the $x = 0.3$ phase, the irreversibility decreases in both (χ') and (χ'') as the field increases and tends to disappear at about $H_{dc} \approx 2000$ Oe (see inset in figure 7). However, the field dependence of the in-phase χ' component for $Co_{1.9}Ni_{0.1}$ shows an unusual magnetic behaviour with several splits of the signal with the applied field (see figure 7). This complex behaviour is not satisfactorily explained by considering that, in a high field, the magnetic energy becomes sufficient to overcome the energy barrier (or blocking temperature) between the possible equilibrium positions of the magnetic moments.

The frequency shifts of the maxima in the χ' susceptibility yield ratios $\Delta T_f/[T_f \Delta(\log \nu)]$ of 0.0058 and 0.048 for $Co_{1.9}Ni_{0.1}$ and $Co_{1.7}Ni_{0.3}$, respectively. The value of

$Co_{1.9}Ni_{0.1}(OH)PO_4$ is similar to that found in $Co_2(OH)PO_4$ (0.0055), whereas that corresponding to $Co_{1.7}Ni_{0.3}(OH)PO_4$ is ten times larger but still within the order of magnitude of those typically found in spin glasses. Assuming a Gaussian variation of the $\chi'(T)$ around T_f, we can determine the position of the maximum (T_f) precisely for each frequency. The frequency dependence in both compounds agrees with the empirical Vogel–Fulcher law $\nu = \nu_0 \exp[-\frac{E_a}{T_f - T_0}]$, characteristic of the spin glass transition. Fits to this law, using the typical value of $\nu_0 = 10^{13}$ Hz [43], are shown as continuous lines in the insets of figure 6. From these fits we obtain reasonable parameters of the activation energy (E_a) and the Vogel–Fulcher temperature (T_0) with $E_a/K_B = 12.5$ K and $T_0 = 10.2$ K for $Co_{1.9}Ni_{0.1}(OH)PO_4$ and $E_a/K_B = 70$ K and $T_0 = 2.8$ K for $Co_{1.7}Ni_{0.3}(OH)PO_4$.

From the observed $C_p(T)$ plot, only one heat capacity peak can be seen at around 65 K in both Co–Ni phases. Although the maximum appears at temperatures slightly lower than those obtained from magnetic measurements, we can get ordering temperatures of $T_N = 64$ and 70 K for $Co_{1.9}Ni_{0.1}$ and $Co_{1.7}Ni_{0.3}$, respectively, if the ordering temperature is defined as the inflection point above the maximum from $C_{p_{mag}}$ data. These results are in good agreement with those obtained from the other techniques. The rapid decrease of $C_{p_{mag}}$ above T_N suggests that short-range order should be small and not have any significant effect on the magnetic behaviour. For $T < T_N$, the estimated magnetic data for the Co–Ni compounds deviate from the ideal behaviour, showing broad anomalies. In any case, the most significant feature in both compounds is the absence of any peak in the low temperature region, confirming the spin glass nature of the low temperature transition.

The magnetic structure of $Co_{2-x}Ni_x(OH)PO_4$ ($x = 0.1, 0.3$) consists of ferromagnetic arrangements between the octahedral chains (sublattice of M(2)) and trigonal bipyramidal dimers (sublattice of M(1)) within the xz plane (see figure 10). The ferromagnetic layers are aligned antiparallel to one another, establishing the three-dimensional antiferromagnetic order through the |OH| and $|PO_4|$ groups. The magnetic moments are aligned along the z axis without changes in the magnetic structures of both compounds below their T_N. In particular, the absence of any changes in the magnetic structure at low temperatures also supports the spin glass nature of the magnetic transition observed in the ac susceptibility around 10 K. It is worth mentioning that the magnetic M(2) moment in $Co_{1.9}Ni_{0.1}$, octahedral site (3.56(8) μ_B), is slightly lower than the one obtained in $Co_2(OH)PO_4$ (Co(2) = 3.84(5) μ_B) due to the strong preference of the Ni(II) ions for the octahedral positions. The component of the refined magnetic moment in the trigonal bipyramidal M(1) of 2.91(9) μ_B shows an unexpected decrease of the value with respect to $Co_2(OH)PO_4$ (Co(1) = 3.39(7) μ_B) that can be attributed to an increase in the frustration in the M(1) positions as a result of the introduction of Ni(II) in the M(2) site. In $Co_{1.7}Ni_{0.3}(OH)PO_4$, the refined M(1) magnetic component is close to that of $Co_{1.9}Ni_{0.1}$, whereas the magnetic M(2) moment decreases significantly (3.19(4) μ_B versus 3.56(8) μ_B). These data indicate that a substitution of approximately 15% of Co^{2+} does not affect the effective magnetic moment in the dimer M(1) positions, the increase in the amount of Ni^{2+} in M(2) being the main factor responsible for the decrease in the average magnetic moment. These results are in good agreement with the structural results obtained at room temperature from the D2B data. Finally, the differences between the octahedral and trigonal bipyramidal sublattices (see figure 12) for $Co_{1.9}Ni_{0.1}$ can be explained by considering that all the magnetic moments in the sublattice M(2) participate in the long range antiferromagnetic order, whereas in the M(1) sublattice only 82% of the moments became ordered contributing the rest to the freezing processes. On the contrary, in the case of $Co_{1.7}Ni_{0.3}$, the magnetic moment in the M(2) positions decreases to become to be lightly higher than those corresponding to M(1) sites due to the presence of 15% Ni(II) in the M(2) position.

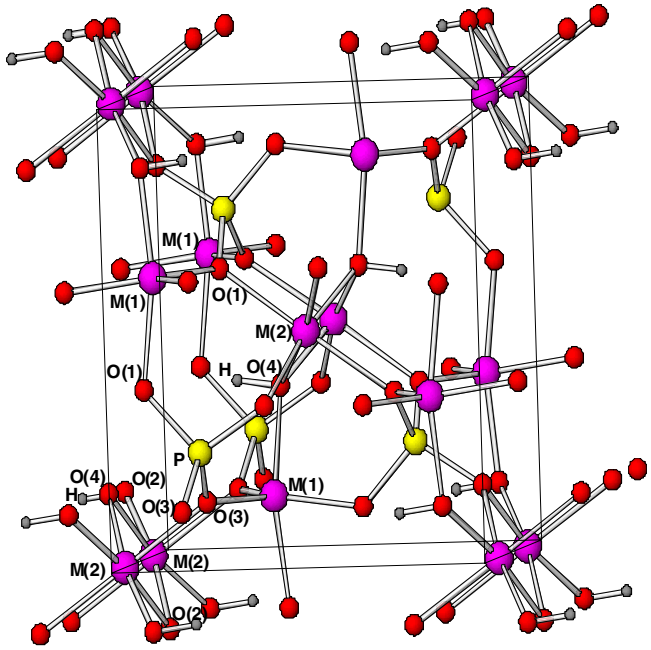

Figure 13. Schematic view of the exchange pathways for $(Co, Ni)_2(OH)PO_4$. Interactions via oxygen bridges and phosphate groups are shown.

The main magnetic exchange pathways present in these compounds are shown in table 4. The shorter metal–metal distances range between 2.9 and 3.7 Å and consequently direct interactions are not negligible. Taking into account that the Ni^{2+} ions prefer the $|M(2)O_6|$ octahedral chains, the substitution of Ni(II) (d^8) ($S = 1$) by Co(d^7) ($S = 3/2$) in the $Co_2(OH)PO_4$ framework [20, 32] modifies the nature of some magnetic interactions. The unpaired electrons in the d_{z^2} and $d_{x^2-y^2}$ orbitals favour the spin frustrations between chains and dimers. Considering the angles in $Co_{1.7}Ni_{0.3}(OH)PO_4$, both ferromagnetic and antiferromagnetic interactions should be observed [44]. A view of the most important exchange pathways in both hydroxyphosphates is given in figure 13, where the solid lines represent connections between M–O–M intradimers and $|M(1)O_5|$ and $|M(2)O_6|$ sublattices. The possible exchange pathways are (i) direct interactions involving M(1) and M(2) sublattices which should lead to antiferromagnetic couplings; (ii) superexchange M–O–M interactions from edge-sharing both in the $[M(1)_2O_6(OH)_2]$ trigonal bipyramidal dimers and $[M(2)O_4(OH)_2]$ octahedral chains whose angles range from 102.0° to 102.6° and from 91.2° to 93.4°, respectively, leading to ferromagnetic interactions (see table 4); (iii) superexchange M(1)–O(3)–M(2) and M(1)–O(4)H–M(2) interactions between dimers and their neighbouring chains that could give rise to ferromagnetic or antiferromagnetic couplings depending on the magnetic exchange angle.

For these compounds, the ferromagnetic interactions observed in the xz plane from neutron data imply a striking exchange angle, M(1)–O(3)–M(2), which ranges between 107° and 108° with two magnetic pathways generated by symmetry. As can be seen, the substitution of up to 15% of Co^{2+} by Ni^{2+} does not affect this orthogonal accidental angle sufficiently to force changes in the sense of the magnetic interactions due to the competition between the magnetic moments. Moreover, the interactions between dimers and chains through the O(4)H are clearly

Table 4. Selected geometrical parameters, bond lengths (Å) and angles (deg) obtained from neutron diffraction and related to the possible magnetic exchange pathways for $Co_{2-x}Ni_x(OH)PO_4$ ($x = 0$, 0.1 and 0.3).

	Direct distance M–M (Å)			Lengh of exchange pathway (Å)		
	$x = 0.3$	$x = 0.1$	$x = 0$	$x = 0.3$	$x = 0.1$	$x = 0$
M(1)–O(1)–M(1)	3.28	2.87	3.24	4.15	3.97	4.17
M(1)–O(1)–P–O(3)–M(1)	5.55	5.62	5.49	7.26	7.36	7.28
M(1)–O(4)H–M(2)	3.64	3.76	3.65	4.13	4.31	4.15
M(1)–O(3)–M(2)	3.55	3.60	3.55	4.37	4.45	4.29
M(1)–O(3)–P–O(2)–M(2)	5.75	5.83	5.64	7.61	7.58	7.38
M(2)–O(4)H–M(2)	2.95	2.90	2.99	4.12	4.16	4.16
M(2)–O(2)–M(2)	3.08	3.14	3.04	4.24	4.23	4.22
M(2)–O(2)–P–O(3)–M(2)	5.64	5.95	6.05	7.34	7.58	7.58

	Angles (deg)											
	M–O–M			M–O–P			O–P–O			P–O–M		
	$x = 0.3$	$x = 0.1$	$x = 0$	$x = 0.3$	$x = 0.1$	$x = 0$	$x = 0.3$	$x = 0.1$	$x = 0$	$x = 0.3$	$x = 0.1$	$x = 0$
M(1)–O(1)–M(1) (F)	102.6	93	102.0									
M(1)–O(1)–P–O(3)–M(1) (AF)				131.3	143	133.0	110.1	105	110.2	133.4	133	131.0
M(1)–O(4)H–M(2) (AF)	123.5	121	123.3									
M(1)–O(3)–M(2) (F)	108.0	107	107.2									
M(1)–O(3)–P–O(2)–M(2) (AF)				133.4	133	133.0	111.1	114	110.2	125.9	124	127.0
M(2)–O(4)H–M(2) (F)	92.4	89	92.5									
M(2)–O(2)–M(2) (F)	93.7	96	93.5									
M(2)–O(2)–P–O(3)–M(2) (AF)				125.8	124	128.6	111.1	114	110.2	117.9	120	112.0

antiferromagnetic, with a mean exchange angle of 123°. The final exchanged pathway is: (iv) superexchange antiferromagnetic interactions through the |OH| and $|PO_4|$ groups, which are linked to the $|M(1)O_5|$ and $|M(2)O_6|$ polyhedra in three dimensions (see figure 13 and table 4). The superexchange M–O–P–O–M interactions, if not totally absent, lead to frustration in the structure which can favour a spin glass type behaviour, as previously discussed. The last pathways allows one to propagate the magnetic interactions giving rise to a three-dimensional magnetic system.

In conclusion, considering the different magnetic exchange pathways with similar exchange angles in both Co–Ni hydroxyphosphates, the existence of magnetic frustration in the M(1) ions present in the dimers, due to the existence of antiferromagnetic interactions between the neighbouring M(2) chains, together with the anisotropy of the Co(II) ions, are responsible for the spin glass behaviour in $Co_{2-x}Ni_x(OH)PO_4$ ($x = 0.1, 0.3$). Furthermore, despite the expected increase in random magnetic interactions with increasing Ni content, the freezing temperature decreases with substitution.

6. Summary

$Co_2(OH)PO_4$ is the first three-dimensional ($T_N \approx 70$ K) antiferromagnetically ordered phosphate with a spin glass state around 15 K. The inequality spin produced by the substitution of Co^{2+} ($S = 3/2$) by Ni^{2+} ($S = 1$) plays an important role in the irreversibility process and their effect on the variations in the properties of the non-substituted phase. In the $Co_{2-x}Ni_x(OH)PO_4$ ($x = 0.1, 0.3$) compounds two Co/Ni crystallographic positions exist. The Ni^{2+} ions are located in the octahedral M(2) chains of the crystal structure with the practical absence of these ions in the trigonal bipyramidal M(1) dimers. An unexpected decrease in the refined magnetic moments with respect to the non-substituted phase was observed. In these compounds spin glass freezing coexists with the long range antiferromagnetic order comprising the freezer moments. The presence of both the strong anisotropy of the Co(II) ions and the magnetic frustration in the M(1) and the neighbouring M(2) sublattices could be the responsible of the complex magnetic behaviour observed in the title compounds. The study of the magnetostructural correlations indicates the important effect of the striking orthogonal accidental angle, M(1)–O(3)–M(2) 108°, on the competition between dimers and chains ensuring cooperativeness of the freezing process associated to a spin glass state.

Acknowledgments

This work was financially supported by the Universidad del País Vasco/EHU (REF 9/UPV00169.310-13494/2001; 9/UPV00130.310-15967/2004), which we gratefully acknowledge. The authors wish to thank the ILL facilities for the provision of beam-time and technical assistance. I de Pedro thanks the Universidad del País Vasco/EHU for a fellowship.

References

[1] Fischer K H and Hertz J 1991 *Spin Glasses* (Cambridge: Cambridge University Press)
[2] Mydosh J A 1993 *Spin Glasses: An Experimental Introduction* (London: Taylor and Francis)
[3] Battlle X and Labarta A 2002 *J. Phys. D: Appl. Phys.* **35** R15
[4] Rivadulla F, Lopez Quintela M A and Rivas J 2004 *Phys. Rev. Lett.* **93** 167206
[5] Magalhaes S G, Schmidt A A, Zimmer F M, Theumann A and Coqblin B 2003 *Eur. Phys. J.* B **34** 447
[6] Marcano N, Espeso J I, Gómez Sal J C, Rodríguez Fernández J, Bartolomé F and Herrero J 2005 *Phys. Rev.* B **71** 134401

[7] Süllow S, Nieuwenhuys G J, Menovsky A A, Mydosh J A, Mentink S A M, Mason T E and Buyers W J L 1997 *Phys. Rev. Lett.* **78** 354
[8] Li D X, Nimori S, Shiokawa Y, Haga Y, Yamamoto E and Onuki Y 2003 *Phys. Rev.* B **68** 172405
[9] Gschneidner K A Jr, Tang J, Dhar S K and Goldman A 1990 *Physica* B **163** 507
[10] Coles B R, Sarkissian B V B and Taylor R H 1978 *Phil. Mag.* **37** 489
[11] Verbeek B H, Nieuwenhuys G J, Stocker H and Mydosh J A 1978 *Phys. Rev. Lett.* **40** 586
[12] Fernandez Barquin L, Gomez Sal J C, Gorria P, Garitaonandia J S and Barandiaran J M 2003 *Eur. Phys. J.* B **35** 3
[13] García Soldevilla J, Gómez Sal J C, Blanco J A, Espeso J I and Rodríguez Fernández J 2000 *Phys. Rev.* B **61** 6821
[14] Nagata S, Keesom P H and Harrison H R 1979 *Phys. Rev.* B **19** 1633
[15] Mulder C A M, van Duyneveldt A J and Mydosh J A 1982 *Phys. Rev.* B **25** 515
[16] Canella V and Mydosh J A 1974 *Phys. Rev.* B **6** 4220
[17] Dubiel S M, Fischer K H, Sauer Ch and Zinn W 1987 *Phys. Rev.* B **36** 360
[18] Wong P Z, Yoshizawa H and Shapiro S M 1985 *J. Appl. Phys.* **57** 3462
[19] Yoshizawa H, Mitsuda S, Aruga H and Ito A 1987 *Phys. Rev. Lett.* **59** 2364
[20] Rojo J M, Mesa J L, Lezama L, Pizarro J L, Arriortua M I, Rodríguez Fernández J, Barberis G E and Rojo T 2002 *Phys. Rev.* B **66** 94406
[21] Hawthorne F C 1976 *Can. Mineral.* **14** 143
[22] Moore P B and Smythe J R 1968 *Am. Mineral.* **53** 1841
[23] Heritsch H 1938 *Z. Kristallogr.* **99** 466
[24] Burnham C B and Buerger M J 1961 *Z. Kristallogr.* **115** 269
[25] Keller P 1971 *Neues Jahrb. Mineral. Monatsh.* **12** 560
[26] Harrison W T, Vaughey J T, Dussack L L, Jacobson A J, Martin T E and Stucky G D 1995 *J. Solid State Chem.* **114** 151
[27] Haushalter R C and Mundi L A 1992 *Chem. Mater.* **4** 31
[28] Clearfield A 1998 *Chem. Rev.* **88** 125
[29] Rapoport W R and Khattaak C P 1988 *Appl. Opt.* **27** 2677
[30] Forrest G T 1989 *Laser Focus World* **25** 23
[31] Rojo J M, Mesa J L, Calvo R, Lezama L, Olazcuaga R and Rojo T 1999 *J. Solid State Chem.* **145** 629
[32] De Pedro I, Rojo J M, Jubera V, Rodríguez Fernández J, Sánchez Marcos J, Lezama L and Rojo T 2004 *J. Mater. Chem.* **14** 1157
[33] Rojo J M, Mesa J L, Pizarro J L, Lezama L, Arriortua M I and Rojo T 1997 *J. Solid State Chem.* **132** 107
[34] Rojo J M, Mesa J L, Lezama L, Barberis G E and Rojo T 1996 *J. Magn. Magn. Mater.* **157** 493
[35] Rojo T, Lezama L, Rojo J M, Insausti M, Arriortua M I and Villeneuve G 1992 *Eur. J. Solid State Inorg. Chem.* **29** 217
[36] Rietveld H M 1969 *J. Appl. Crystallogr.* **2** 65
[37] Rodríguez-Carvajal J 1992 FULLPROF program for rietveld refinement and pattern matching analysis of powder patterns *Physica* B **192** 55 and later unpublished versions.
The program is a strongly modified version of that described by Wiles D B and Young R A 1981 *J. Appl. Crystallogr.* **14** 149
[38] Chernova N A, Song Y, Zavalij P Y and Whittingham S 2004 *Phys. Rev.* B **70** 144405
[39] Debye P 1912 *Ann. Phys., Lpz.* **39** 789
[40] Bertaut E F 1968 *Acta Crystallogr.* A **24** 217
[41] Soukoulis C M, Grest G S and Levin K 1983 *Phys. Rev.* B **28** 1510
[42] Lue C S, Oner Y, Naugle D G and Ross J H 2001 *Phys. Rev.* B **63** 184405 and references therein
[43] Tholence J L 1980 *Solid State Commun.* **35** 113
[44] Goodenough J B 1963 *Magnetism and the Chemical Bond* (New York: Interscience)